Acta Materialia 106 (2016) 171–181

Contents lists available at ScienceDirect

Acta Materialia

journal homepage: www.elsevier.com/locate/actamat

Full length article

Suppression of surface recombination in CuInSe2 (CIS) thin films via Trioctylphosphine Sulfide (TOP:S) surface passivation

Shi Luo [a, *], Carissa Eisler [b], Tsun-Hsin Wong [c], Hai Xiao [d], Chuan-En Lin [c], Tsung-Ta Wu [e], Chang-Hong Shen [e], Jia-Min Shieh [e], Chuang-Chuang Tsai [f], Chee-Wee Liu [g], Harry A. Atwater [b], William A. Goddard III [d], Jiun-Haw Lee [c], Julia R. Greer [a]

[a] Division of Applied Science and Engineering, California Institute of Technology, USA
[b] Thomas J. Watson Sr. Laboratory of Applied Physics, California Institute of Technology, USA
[c] Graduate Institute of Photonics and Optoelectronics and Department of Electrical Engineering, National Taiwan University, Taiwan, ROC
[d] Materials and Process Simulation Center, California Institute of Technology, USA
[e] National Nano Device Laboratories, Taiwan, ROC
[f] Department of Photonics and Institute of Electro-Optical Engineering, National Chiao Tung University, Taiwan, ROC
[g] Department of Electrical Engineering, National Taiwan University, Taiwan, ROC

ARTICLE INFO

Article history:
Received 16 December 2015
Accepted 8 January 2016
Available online 21 January 2016

Keywords:
CuInSe2 (CIS) solar cells
Thin film passivation
Na diffusion
DFT calculations
STEM-EDS

ABSTRACT

CuInSe2 (CIS) solar cells are promising candidates for thin film photovoltaic applications, one key limitation in their performance is surface recombination in these thin films. We demonstrate that passivating CIS films with Trioctylphosphine Sulfide (TOP:S) solution increases photoluminescence (PL) intensity by a factor of ~30, which suggests that this passivation significantly reduces surface recombination. X-ray photoelectron spectroscopy (XPS) reveals that TOP:S forms both −S and −P bonds on the CIS film surface, which leads to a ~4-fold increase in the surface Na peak intensity. This value is significantly higher than what would be expected from high temperature annealing alone, which has been linked to improvements in surface morphology and device efficiency in CIGS solar cells. We use Energy-Dispersive X-ray Spectroscopy (EDS) to measure the solid-state transport of Na within CIS films with and without passivation. EDS spectra on CIS film cross-sections reveals a saddle-shaped Na profile in the as-fabricated films and a concentration gradient towards the film surface in the passivated films, with 20% higher surface Na content compared with the unpassivated films. We employ Hybrid (B3PW91) Density Functional Theory (DFT) to gain insight into energetics of Na defects, which demonstrate a driving force for Na diffusion from bulk towards the surface. DFT Calculations with TOP:S-like molecules on the same surfaces reveal a ~ 1eV lower formation energy for the Na_{Cu} defect. The experiments and computations in this work suggest that TOP:S passivation promotes Na diffusion towards CIS film surfaces and stabilizes surface Na defects, which leads to the observed substantial decrease in surface recombination.

1. Introduction

$CuInSe_2$ (CIS) and $Cu(In,Ga)Se_2$ (CIGS)-based solar cells are among the most promising candidates for thin film photovoltaics [1], with efficiencies over 21% recorded for CIGS cells on soda lime glass (SLG) substrates [2] and over 18% on polyimide [3]. One key factor that has been shown to improve the efficiency of such compound semiconductor devices is passivating the top and bottom of the semiconductor surfaces, which can suppress minority carrier recombination near the surface [4–6]. An Improved open circuit voltage (V_{oc}) and an efficiency of up to 30% have been reported for Al_2O_3 passivated CIGS thin film solar cells [5,7].

This work demonstrates that passivating the CIS surface with Trioctylphosphine Sulfide (TOP:S) ($SP(C_8H_{17})_3$) provides dramatic improvement in the minority carrier surface recombination. TOP:S has been previously shown to be a viable material for passivating surface flaws in nano-crystals [8], and TOP:S passivation has been reported to protect scribed CIGS thin films from surface and edge defects, which leads to up to 40× enhancement in photoluminescence (PL) intensity and ~25% improved device efficiency

* Corresponding author. 1200 E., California Blvd., MC 309-81, Pasadena, CA91125, USA.
E-mail address: slluo@caltech.edu (S. Luo).

http://dx.doi.org/10.1016/j.actamat.2016.01.021
1359-6454/

[9]. X-ray photoelectron spectroscopy (XPS) analysis on passivated CIGS films revealed a greater than 3× increase in the Na peak, which suggests higher Na content in the surfaces of TOP:S-coated films [9].

Na plays an important role in the operation and performance of CI(G)S solar cells, where incorporating less than 1.0 at.% Na can increase both the V_{oc} and the short circuit current density (J_{sc}) of CI(G)S solar cells by up to 30%, improve device efficiency by up to 20%, govern grain growth during CI(G)S film deposition, and lead to smoother surface morphology [10–14]. It is common for Na to diffuse into the CI(G)S films from the SLG substrate, after which it resides primarily within the grain boundaries. The mechanism for Na incorporation into CI(G)S is not fully understood; reports on Na distribution and its effect in CIS and CIGS films have been inconsistent [11,15]. For example, the higher Na concentration at the film surface and at grain boundaries in CIGS revealed by energy-dispersive X-ray spectroscopy (EDS) and atom probe tomography measurements has been attributed to grain structure improvements and efficiency enhancement by up to 25% [12,16–18]; other studies using secondary ion mass spectroscopy (SIMS) showed a negligible presence of Na within the CIS films and associated excess surface Na content leading to deteriorating surface morphology [19].

We combine experiments and theory to explore the effect of TOP:S passivation on CIS thin films and on the incorporation and diffusion of Na within the CIS system. We focus on CIS as a model system in the experiments and in the density functional theory (DFT) computational analysis. The similarities in the microstructure and lattices of CIS and CIGS lead to their nearly-equivalent material properties [20]. Conventional Density Functional Theory is often thought to predict inaccurate band gaps and band offsets for semiconductors such as CIS [21], however we showed previously that using the B3PW91 hybrid functionals predicts a band gap of 1.05 eV for CIS and systematically leads to band offsets within 0.09 eV of experiment [21,22], rendering this type of DFT most useful in studying the surface passivation effects and Na diffusion.

2. Methods

2.1. Sample preparation

1200 nm-thick CIS films were deposited at National Nano Device Laboratories (NDL) of Taiwan by the following procedure: (1) 500 nm molybdenum back electrodes were sputtered on Soda Lime Glass (SLG) substrate by a two-steps process (high working pressure followed by low pressure) at room temperature. (2) Cu and In metal precursors were multi-layered sequentially onto the Mo layer and annealed without Se vapor at annealing temperature of 330 °C (3) The annealed Cu/In mixture was processed via hydrogen assisted solid Se vapor selenization (HASVS) with N_2(85%)/H_2(15%) carrier gas at 550 °C [23,24]. This fabrication method was chosen over other methods that yield higher efficiencies, such as three-stage co-evaporation of CIGS thin films for its better scalability. The total thickness of the CIS absorber layer was measured via scanning electron microscopy (SEM) to be 1.2 ± 0.1 μm. At this point the finished CIS wafer was cut in half, with one half immersed in TOP:S solution for 24 h at 120 °C and the other left as-is.

For passivation of CIS thin films, the samples were immersed in TOP:S solution in a glove box (O_2 and H_2O ~200 ppm) for up to 48 h under different temperatures (RT, 80 °C and 120 °C), followed by a 10 min toluene rinse to remove the excess TOP:S [4].

Transmission electron microscopy (TEM) samples of CIS film cross-sections were created by mechanical polishing followed by low-angle Ar ion milling using Fischione Model 1050 TEM mill. TEM sample thickness was measured under SEM (FEI VERSA Dual-beam) to be 50–80 nm.

2.2. Experimental

SEM and TEM images are taken in FEI VERSA Dual-beam SEM/FIB and FEI Tecnai TF-30 TEM respectively. Grain sizes were estimated based on the SEM and TEM images in the following manner: (1) multiple lines of the same length were drawn across the image in both horizontal and vertical directions emanating from different, randomly chosen points; (2) number of intersections of the lines with the grain boundaries were recorded; (3) the average grain size is taken to be the total length of the lines divided by the total number of intersections. For PL measurements, the CIS samples were excited by a 671 nm pumping laser and the photoluminescence signal was collected by a monochromator and InGaAs photodetector connected to a lock-in amplifier. XPS measurements were conducted with a Kratos surface-science instrument and an Al Kα (1486.7 eV) x-ray source under high vacuum (1 × 10–9 torr). The ionization potential of CIS thin films under air was measured by a photoelectron spectrometer (AC-2, Riken Keiki). EDS analysis was conducted using FEI Tecnai TF-30 transmission electron microscope in scanning transmission electron microscopy (STEM) mode, using an acceleration voltage of 300 kV and live acquiring time of 300 s for each measurement. Quantitative atomic percentage (at.%) analysis was carried out using Oxford INCA Energy EDS X-ray Microanalysis System. Density of CIS films was taken as stoichiometric $CuInSe_2$ as 5.77 g/cm [25]. Five measurements were taken at each location: one measurement from a rectangular area of~70nm × 70 nm, followed by point measurements at the four corners of the rectangle. The size of the measured area is chosen to minimize the effect of local inhomogeneity such as grain boundaries.

2.3. Computation details

The DFT calculations used the Hybrid functional B3PW91 [26] that we have shown to provides accurate bandgaps [21] and band offsets [22] (average mean error of 0.09 eV) for chalcopyrite semiconductors. Thus B3PW91 leads to a band gap of 1.05 eV for CIS compared to 1.04 eV from experiment and <1 eV from typical DFT methods (Perdew-Burke-Ernzerhof, PBE) [21]. To accurately represent the small Na contents, we used periodic unit cells with 64 atoms. Hybrid B3PW91 calculations are not practical for DFT codes (such as VASP and Quantum Expresso) that use standard plane wave basis sets (1000s of times slower than PBE). Consequently we use local atomic Gaussian-type basis sets that enables fast evaluation of the Hartree–Fock exchange terms [27]. As implemented in the CRYSTAL09 [27] software package, B3PW91 is only 1.7 times the cost of PBE, while about 2 orders of magnitudes faster than PBE in VASP [21].

Optimized Cu, In, Se and Na basis sets and pseudopotentials were taken from our previous work [22]. For each system we relaxed the structure until the forces on each atom dropped below 4.5×10^{-4} Hartree/Bohr. For Cu, In and Se, we used the SBKJ relativistic angular momentum projected effective core potentials [28,29] and associated basis set [30], while for Na atoms and the $SP(CH_3)_3$ molecule we used a complete all-electron basis set. Following Xiao et al. [22], we did not include Spin-orbit Coupling (SOC) since all the systems considered here are closed-shell (no unpaired spins). We used an extra-large k space grid to ensure accurate integration, and we used the Γ-centered Monkhorst-Pack scheme [31] to sample reciprocal space with a resolution of ~ $2\pi \times 1/40$ Å^{-1}.

We kept the number of Se atoms per periodic cell constant at 32 for all bulk ($CuInSe_2$) and surface ($CuInSe_2$ and $Cu_5In_9Se_{16}$)

calculations.

For surface calculations, free surfaces of $CuInSe_2$ and $Cu_5In_9Se_{16}$ were cleaved from respective bulk unit cells and relaxed prior to introduction of Na defects.

Calculations with SP(CH3)3 molecules were started by placing the molecule at 2 Å above the free surface with S atom adjacent to the Cu substitution site, and S═P bond parallel to the surface normal. The system was then fully relaxed before the atom on the Cu site was replaced with Na, at which point the system was allowed to relax again.

3. Results

3.1. Surface measurements of TOP:S passivated CIS films

Fig. 1 shows the PL intensity of CIS films with different passivation times (Fig. 1(a)) and different passivation temperatures (Fig. 1(b)), each normalized by the PL intensity of as-fabricated films. All PL peaks were found to be at ~0.96 eV without any obvious spectral shifts. For the passivation temperature of 120 °C, the normalized intensity increased with passivation time and peaked after 24 h at ~29 times higher than the baseline. The intensity remained relatively the same for longer passivation times, reaching a 32.7 times increase over the baseline after 48 h. For the fixed passivation time of 24 h, varying the passivation temperature from room temperature (RT) to 80 °C and 120 °C led to factors of 2.5, 6.2, and 29 times enhancements in PL intensity respectively, which demonstrates that PL response is a strong function of solution treatment temperature.

XPS measurements were conducted on CIS films with and without the TOP:S passivation at room temperature to understand the binding state of TOP:S on passivated film surfaces. Fig. 1(c) shows the XPS peaks of S 2*p* (161.8 eV), Se $3p_{1/2}$ (166.1 eV), and $3p_{3/2}$ (160.5 eV); Fig. 1(d) shows the XPS peak of P $2p_{3/2}$ (133.1 eV) and the Auger peak of Se. These spectra reveal the emergence of a small S 2*p* peak after passivation, which indicates that the sulfur from TOP:S binds to the film surface, presumably by forming Cu_2S and In_2S_3. Fig. 1(d) shows an increase in the P *2p* peak as a result of the P atom in the TOP ligand interacting with dangling bonds on the film surface. In contrast to the increases in PL intensity, the increases in the intensity of S and P XPS peaks were independent of TOP:S passivation temperature (see supporting information, SI), which suggests that binding of TOP:S molecules to the film surface did not cause the increase in PL.

Fig. 2(a) shows surface XPS measurements of the Na *1s* peak (1074 eV) intensity of the samples that were passivated for different durations, normalized by intensity of as-fabricated films. It shows a ~4.5× increase in the Na *1s* peak intensity for samples that were passivated in TOP:S solution for 24 and 48 h, which indicates a significantly higher surface Na content in passivated films. This correlates well with the observed increase in the PL peak intensity over the same passivation times; with the system reaching full saturation after 24 h (Fig. 1(a)). Varying the processing temperatures of the TOP:S treatment for the fixed time of 24 h led to a monotonic increase in the same Na peak, which also correlates with the trends in PL enhancement (Fig. 1(b)). We treated some of the samples with TOP:S and trioctylphosphine (TOP) at 120 °C for 24 h in addition to annealing in Se free atmosphere at 600 °C for 12 h to determine whether the surface Na content increase might have been caused solely by the high-temperature annealing of the film on the SLG substrate. The 600 °C annealing temperature mimic typical high temperature selenization processes and was selected

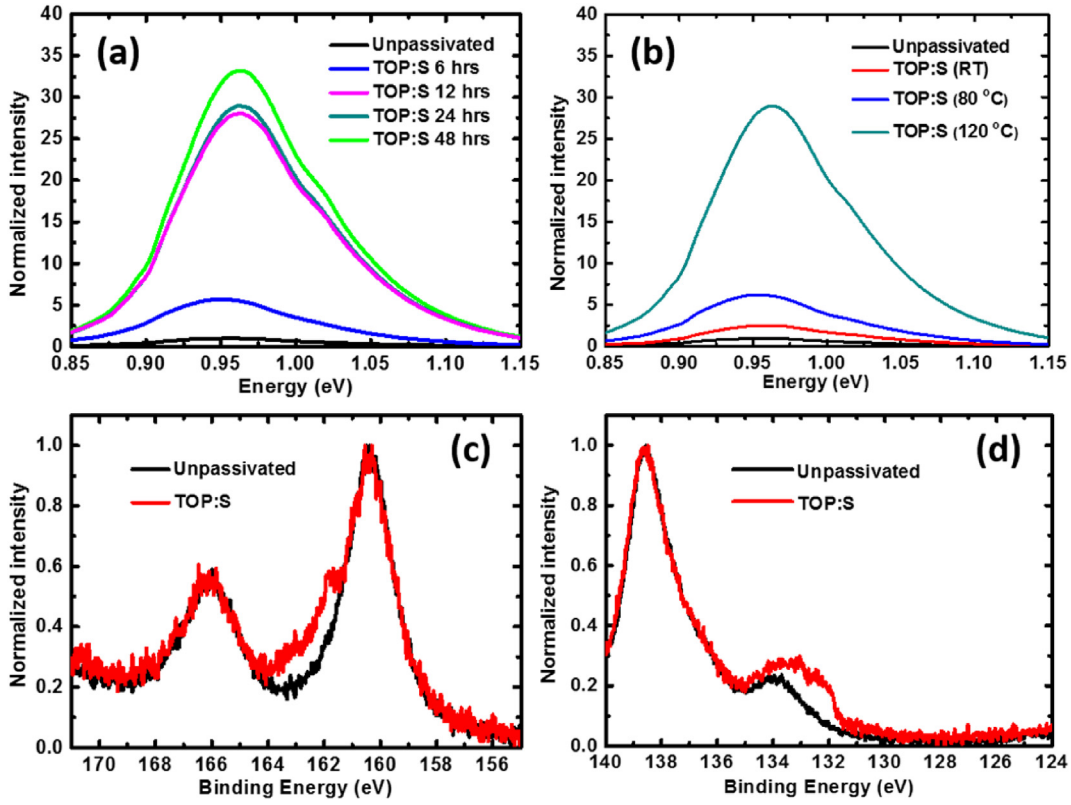

Fig. 1. (a) Normalized PL intensity for unpassivated (baseline) CIS films, and films with passivation times up to 48 h. (b) Normalized PL intensity for unpassivated (baseline) CIS films, and films for passivation temperature up to 120 °C. (c,d) Surface XPS spectra of (c) S 2s and (d) P 2p peaks for CIS thin films with (red) and without (black) TOP:S treatment (120 °C, 24 h). (For interpretation of the references to colour in this figure legend, the reader is referred to the web version of this article.)

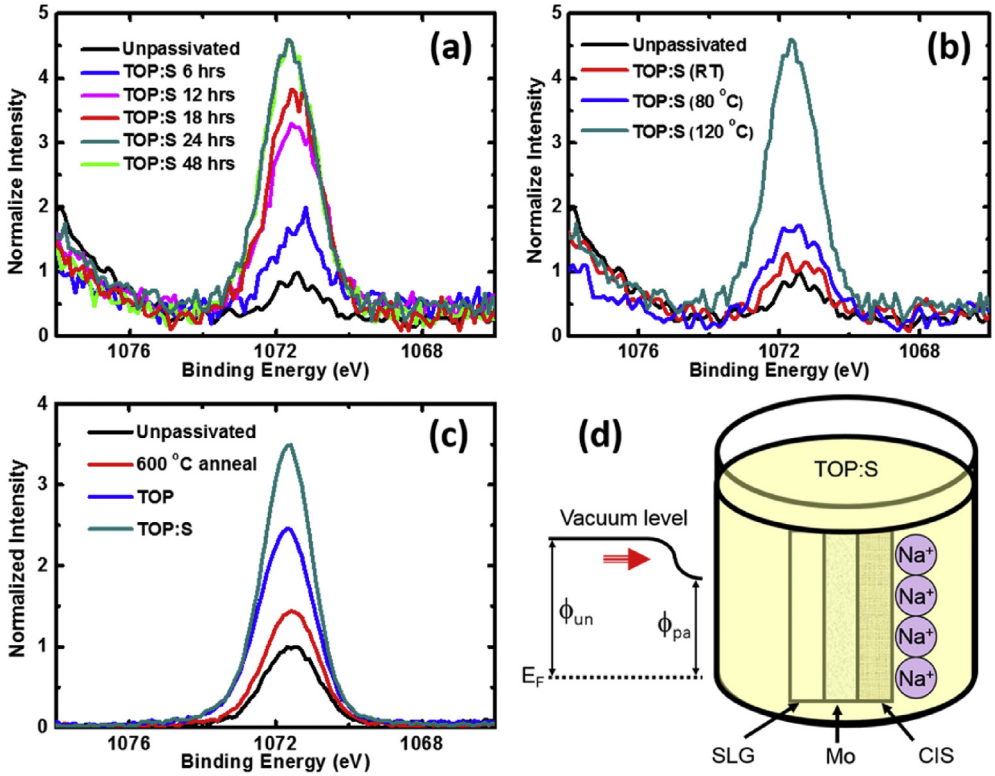

Fig. 2. Surface XPS spectra of Na *1s* peak for unpassivated CIS film (baseline) and (a) films with passivation times up to 48 h, (b) films with passivation temperatures up to 120 °C, and (c) SLG substrates treated with TOP and TOP:S at 120 °C for 24 h and annealed at 600 °C for 12 h. (d) Schematic of increased surface Na concentration from TOP:S passivation, and the alteration of energy levels.

to amplify potential temperature effect on surface Na content, as no noticeable change was observed in reference samples annealed at 120 °C. Fig. 2(c) shows that the ~2.5x- and 3.5x-higher Na concentration in the TOP and TOP:S-treated samples was significantly higher than that in the annealed samples, ~1.3×. It has been proposed that Na concentration at CIS surface leads to shifts in surface energy levels. Surface ionization potential (Fig. S4) show a distinct energy level shift in TOP:S passivated films, which is in accordance with our previous DFT calculations [22]. Fig. 2(d) shows Na congregates at CIS film surface in TOP:S solution and the resulting change in surface ionization potential.

3.2. Analysis of through-thickness Na concentration profile

Fig. 3 shows two scanning transmission electron microscopy (STEM) images of (a) as-fabricated and (b) passivated CIS films overlaid with quantitative EDS measurements of Na content at each location. These images show that the TOP:S passivation did not introduce visible changes to surface morphology of the films. Parts of the passivated film (Fig. 3(b)) near the surface delaminated and adhered to the epoxy layer applied during TEM sample preparation. This is likely a result of residual stress introduced into the underlying film by the passivation process, a common side effect of thin film passivation [4]. The STEM images show a non-uniform grain size distribution in both films; transmission electron microscopy (TEM) analysis revealed that the grain size in both films ranged from 50 to 800 nm, with an average of 305 nm and a standard deviation of 210 nm. Multiple voids were observed in both films at a distance of ~100 nm above the Mo layer, consistent with previous work on a similar material system [32]. EDS analysis indicates that the average surface content of Na increased from 0.99 ± 0.20 at.% in the as-fabricated films to 1.11 ± 0.11 at.% in the passivated films. These concentrations are consistent with reports on atomic probe tomography measurements of Na at grain boundaries within CIS films [16,17], and are higher than some previously reported surface measurements [11]. This discrepancy can be attributed to the limited resolution of most surface techniques like EDS and secondary ion mass spectrometry (SIMS), and the high temperature deposition steps such as the selenization process at 550 °C and the annealing process at 330 °C, which have been shown to increase surface concentration of Na [24]. We found a distinct concentration gradient present in passivated films, with Na content of 0.41 ± 0.09 at.% at the Mo/CIS film interface and 1.11 ± 0.11 at.% at the surface of the film. In the as-fabricated films (Fig. 3(a)), the Na content of the film is higher at (0.78 ± 0.10 at.%) near the Mo interface, then decreases to 0.20 ± 0.06 at.% midway through the film, and increases to 0.99 ± 0.20 at.% at the film surface. EDS area maps of Cu, In, Na and Se for passivated and as-fabricated films can be found in Figs. S2 and S3 in SI. The low overall concentration of Na and the increased background noise from large area map measurements render these concentration profile maps less useful for quantitative analysis compared to point measurements.

3.3. Energetics of Na defect formation in bulk CIS

We conducted DFT calculations to investigate the energetics of Na defects in CIS films. Fig. 4(a) shows a schematic of 4 different types of Na defects in bulk CIS analyzed in this work: (1) Substitutional Na on a Cu lattice site (Na_{Cu}), (2) Substitutional Na on an In lattice site (Na_{In}), (3) Na in a tetrahedral interstitial site within the CIS lattice (Na_{tet}), and (4) Na in an octahedral interstitial site within the CIS lattice (Na_{oct}). In the simulations, a single Na atom was introduced into a 64-atom $CuInSe_2$ unit cell, which corresponds to a Na defect density of 1.3 at.%, a magnitude similar to the surface

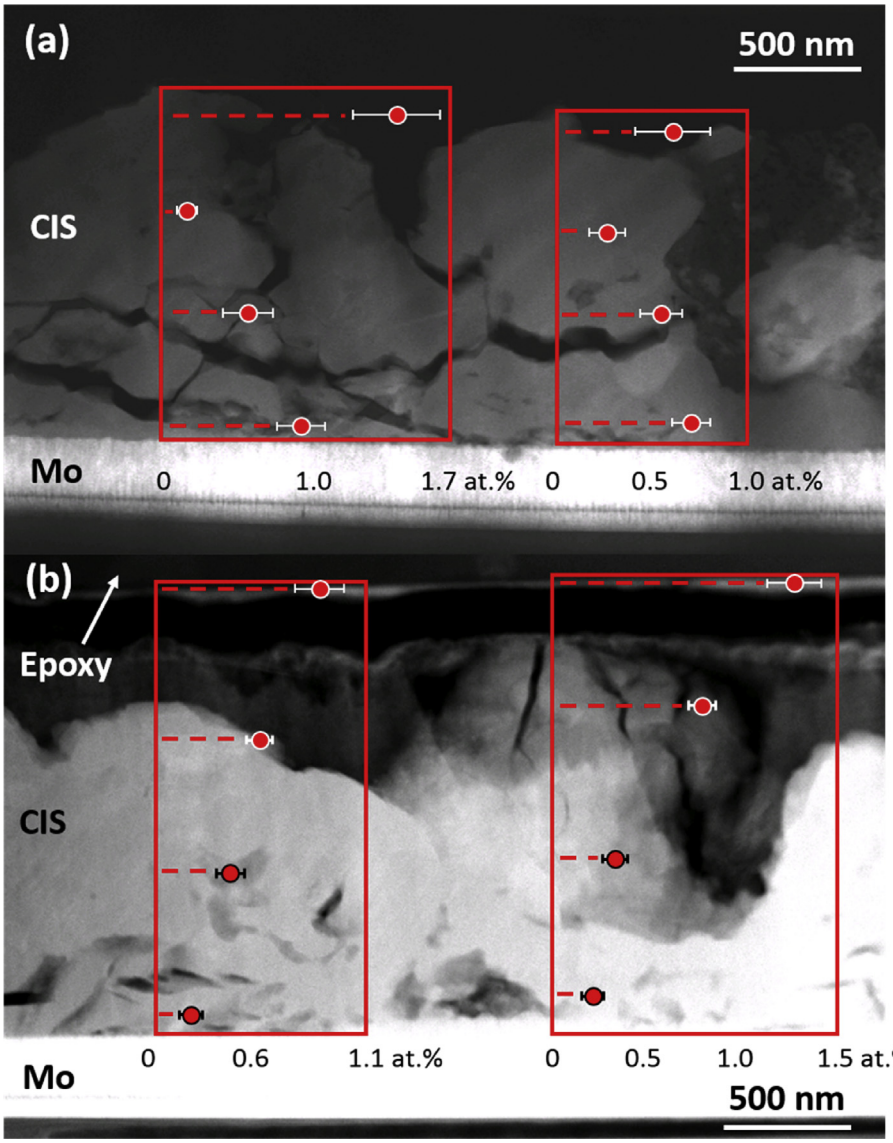

Fig. 3. Representative cross-sectional STEM images with Na concentration profiles overlaid over the images for (a) as-fabricated and (b) TOP:S passivated CIS films. The intercepts between the dashed lines with boxed regions show the actual location of the measurements. The x-axis shows the average Na content (at.%) based on 5 different measurements at each location.

concentration measured by EDS. All calculations in bulk CIS crystals are performed in stoichiometric $CuInSe_2$ systems. We did not consider Na–Na "dumbbells," where two Na atoms reside on the same lattice site, in these simulations because their formation energy at various sites has been reported to follow the same trend as their single-atom counterparts [33].

We represent and compute the total defect formation energy E_F by:

$$E_F = E_{defect} - E_{bulk} \pm \sum \overline{n}_i \mu_i + qE_{Fermi} \quad (1)$$

where E_{bulk} is the total energy of the bulk unit cell, E_{defect} is the total energy of the unit cell that contains the specific defect, μ_i and $\overline{n}_i$ are the chemical potential and the concentration of species i, q is the defect charge state derived from the differences in charge states for individual species (+1 for Cu and Na, +3 for In), and E_{Fermi} is the system Fermi level relative to the valence band maximum (VBM). We calculated the product $\overline{n}_i\mu_i$ for Cu and In as the energy of removing one Cu or In atom from the bulk unit cell, respectively. This product, $\overline{n}_i\mu_i$ for Na as a point defect in the CIS system is not as readily available because Na is extrinsic to the system. Previously, Wei et al. and Oikkonen et al. approximated this potential by extrapolating the potential for bulk body-centered cubic (BCC) Na and Na–In–Se compounds [13,33]. We chose not to use this approach because it is not able to capture the changes in the Na potential with respect to Cu content, which is critical to our investigation of Na_{Cu} defects. Instead, we calculated the total energy of different CIS systems with variable Na contents, where Na atoms were introduced into the systems as Na_{Cu} substitution. We investigated CIS systems with varying unit cell sizes: (1) 32-atoms, (2) 64 atoms, (3) 128 atoms, and (4) 256 atoms; in each case 1 Cu atom on the lattice was replaced with a Na atom. The systems were relaxed in similar a fashion to the bulk calculations detailed above. The $\overline{n}_{Na}\mu_{Na}$ term in Eq. (1) that represents the energy difference of Na_{Cu} substitution defect at various Na concentrations can now be extrapolated from the plot of total system energy vs. Na–Cu substitution content in Fig. S5. It is reasonable to assume that within the same concentration range for Na, its potential in a Cu-lattice site

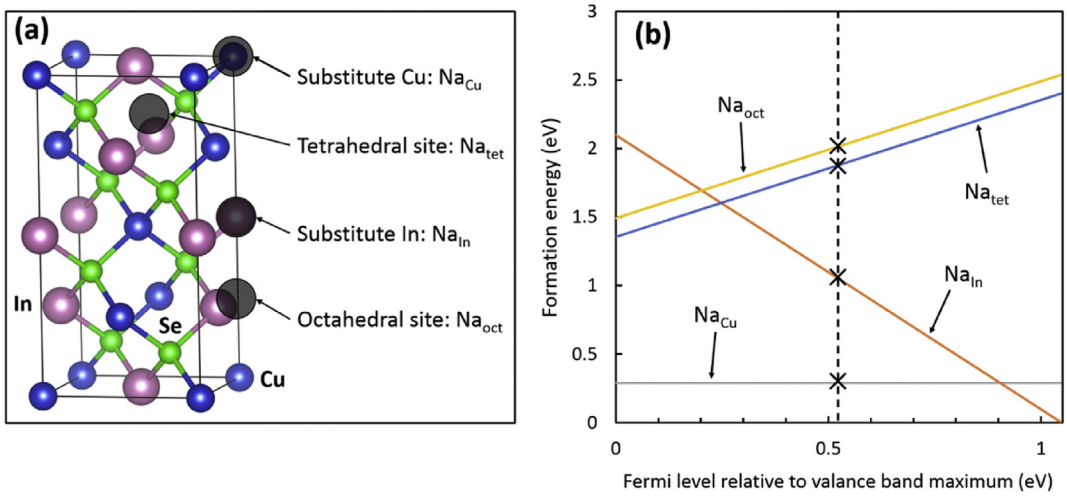

Fig. 4. (a): Schematic showing various Na defects in the CIS unit cell, Na atoms are shown in black, Cu in blue, In in red, and Se in green. (b): Formation energy (eV) of various Na defects as a function of Fermi energy (eV) relative to VBM. Intercepts with the dashed line marks formation energies at intrinsic Fermi level. (For interpretation of the references to colour in this figure legend, the reader is referred to the web version of this article.)

is comparable to that in an In-lattice or in an interstitial site. The difference in energy for other forms of Na point defects can be obtained by modifying the energy difference for Na_{Cu} with chemical potentials of Cu and In in CIS system.

To account for different doping conditions in CIS films, the Fermi level of the system was allowed to vary across the calculated bandgap of 1.05 eV [22], which is consistent with experiments [34,35] and simulations [33,36]. The calculated bandgap value is used here to benchmark against previous calculations such as Oikkonen et al. who reported Na_{Cu} formation energy ~ -1eV, because absolute values for formation energy often significantly depend on alignment of system Fermi level, whereas system bandgap is a better representation of accuracy of calculation. Defect formation energies as a function of Fermi level are plotted in Fig. 4(b), where the intercepts with the solid vertical line marks the mid-bandgap formation energy (0.52 eV from VBM). These results indicate that Na at a Cu lattice site, $Na_{Cu,}$ has the lowest formation energy among all the defects types considered under most doping conditions; Na at an In lattice site, $Na_{In,}$ becomes favorable under extreme n-type doping, where the Fermi level shifts to 0.9 eV above VBM.

3.4. Calculation of Na_{Cu} energetics at the film surface

We used DFT to calculate the formation energies of Na defects in the CIS film surfaces. It has been reported that CIS surfaces could facet into polar [112] orientations from the non-polar [110] orientation to minimize the surface free energy [37]. This is consistent with experimental observations of faceted surfaces in CIS and CIGS films in our previous work [32]. Surface Cu content has significant impact on device performance of CIS thin film solar cells. An artificial Cu-deficient surface condition is often enforced as it has been reported to improve device efficiency and open circuit voltage by up to 25% [20,24]; while a higher surface Cu content has also been shown to reduce surface defect and improve uniformity [38,39]. Here we investigated surfaces with both stoichiometric and deficient Cu content. Similar to our previous DFT studies on CIGS [22], we simulated the Cu-deficient condition with the $Cu_5In_9Se_{16}$ unit cells (Cu content 17 at.%, designated by Cu-poor) obtained by removing some of the Cu atoms from the stoichiometric $Cu_1In_1Se_2$ unit cells (Cu content 25 at.%, designated by Cu-rich) and inserting additional In atoms in their place if needed to balance the charge, while maintaining the total number of Se atoms constant. We constructed all unit cells consistent with these compositions and chose the geometry with the lowest DFT energy as the optimal structure. We considered Cu rich and Cu-poor conditions for both surface orientations, a total of 4 cases: (1) Cu-rich (110), (2) Cu-rich (112), (3) Cu-poor (110) and (4) Cu-poor (112). Our calculations demonstrate that of all possible defect occupancy sites, the sodium-copper substitution, Na_{Cu} is the most energetically favorable defect in bulk CIS (Fig. 4(b)). We postulate that it is also the preferred type of defect at the CIS surface because the vicinity of the free surface is unlikely to change the electron configuration of substitutional point defects in the case of Na_{Cu} and sodium-indium substitution $Na_{In,}$ [22] while interstitial Na defects are significantly higher in formation energy compared to substitutional cases. Based on these findings, we restrict surface calculations to Na_{Cu} only; and the defect charge state q in Eq. (1) becomes 0 because Na and Cu are monovalent, and the term qE_{Fermi} vanishes.

To investigate the interactions between TOP:S passivation and the surface Na defects, we conducted additional DFT simulations: (1) A small organic molecule $SP(CH_3)_{3,}$ used to represent the TOP:S, was placed on top of the cleaved CIS surfaces with various Cu contents and orientations (Fig. S6). The sulfur-phosphorus double bonds (S=P) in the $SP(CH_3)_3$ molecules were aligned along the surface normal, with the S atom adjacent to the surface. The molecule was placed 2 Å away from a Cu atom closest to the surface. The model molecule, $SP(CH_3)_3$, has shorter carbon chains than TOP:S ($SP(C_8H_{17})_3$), the additional carbon atoms in TOP:S have a negligible effect on the electron distribution of S and P atoms, and it is unlikely that the carbon chains interact directly with the CIS surface. It is reasonable to consider $SP(CH_3)_3$ and TOP:S as equivalent in their effects on surface defect energetics and will be referred to them interchangeably from now on. (2) The system was then fully relaxed, and some of the Cu atoms were replaced with Na to form the Na_{Cu} substitution. (3) The Na-containing, "passivated" films were then fully relaxed using DFT similar to bulk calculations, and the formation energy of Na_{Cu} was calculated using Eq. (1). Fig. 5 shows a schematic for calculating the formation energy of Na_{Cu} in the presence of $SP(CH_3)_3$ for stoichiometric (110)-oriented CIS films.

Fig. 6 shows the formation energies of Na_{Cu} for each of the 4 surface cases, with and without passivation. This plot reveals that the formation energies of all unpassivated surfaces (blue bar) are lower (more stable) compared to those energies in the bulk, with

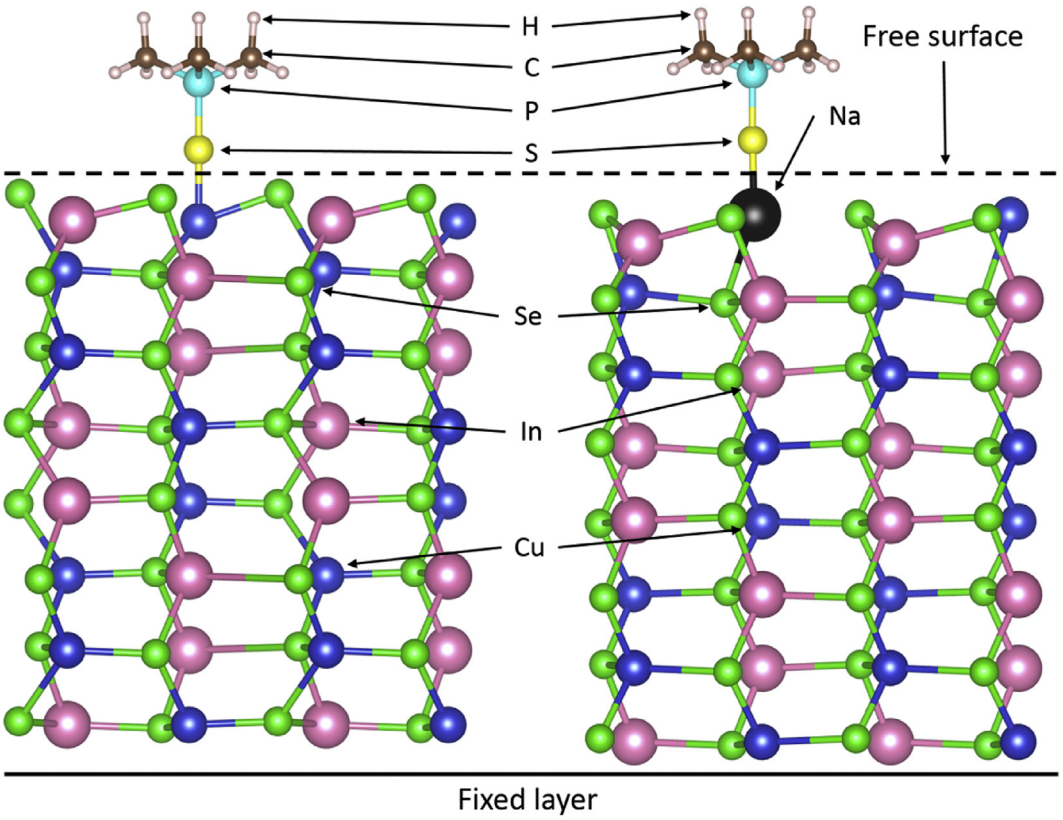

Fig. 5. Left: Optimized CIS unit cell with one $SP(CH_3)_3$ placed on top. Cu atoms are shown in blue, In in red, Se in green, S in yellow, P in cyan, C in brown, and H in white. Right: Optimized CIS unit cell with one Na_{Cu} substitution and one $SP(CH_3)_3$ placed on top of the Na atom. The Na atom is shown in black. In both schematics dashed line shows the direction of the free surface, and the solid line shows the direction of fixed atomic layer. (For interpretation of the references to colour in this figure legend, the reader is referred to the web version of this article.)

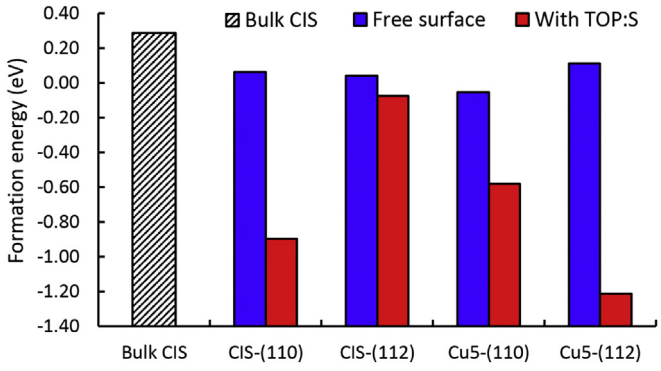

Fig. 6. Shaded: Formation energy (eV) of Na_{Cu} substitution in bulk CIS taken from Fig. 4(b). Blue: Formation energy (eV) of Na_{Cu} substitution on different surfaces (Cu-poor $Cu_5In_9Se_{16}$, Cu-rich $Cu_1In_1Se_2$, (110) and (112) orientations). Red: Formation energy (eV) of Na_{Cu} substitution on the same surfaces with one $SP(CH_3)_3$ placed on top. (For interpretation of the references to colour in this figure legend, the reader is referred to the web version of this article.)

distinct differences among different surface conditions. Cu-poor (110) surfaces have the lowest (most favorable) formation energy at −0.05 eV, compared to 0.29 eV in the bulk. A comparison with passivated surfaces (red bar) reveals that the formation energies decrease for all surface configurations after passivation. Here significant decreases up to ~1 eV were reached for Cu-rich (110) and Cu-poor (112) cases. In all cases, the surface formation energies of Na_{Cu} are lower compared to those in the bulk, suggesting the presence of a driving force for Na diffusion towards film surfaces, which is further enhanced by TOP:S passivation. Fig. 7 shows the atomic-level configurations of the Na defect within each CIS film surface studied, as well as the passivation molecule after surface relaxation.

4. Discussion

4.1. Na distribution in the presence of TOP:S passivation

Surface passivation in semiconductors is commonly used to eliminate surface defects and flaws, such as vacancies and interstitials, which is often manifested by higher carrier density and surface PL intensity [5,7,9,40]. Fig. 1(a) shows that the PL intensity increases by ~29 times with passivation time up to 24 h and remains relatively constant with longer passivation duration, which suggests that the surface is fully saturated with the TOP:S molecule. Such an increase is in accordance to previous reports on passivation of CI(G)S samples from similar deposition conditions [9], and can be attributed to the relatively poor surface uniformity and morphology of the CIS samples tested. It shows that the TOP:S solution treatment passivates the existing surface defects and leads to a reduction in surface recombination, reaching full saturation after 24 h Fig. 1(b) shows that the enhancement in PL increases monotonically with higher treatment temperatures, which suggests that the passivation effect may involve a temperature-limiting process, such as solid-state diffusion [4]. XPS surface analysis of the same samples (Fig. 1(c), d) reveals higher S and P peaks on the film surfaces, likely caused by the formation of Cu_2S and In_2S_3 and the interaction between the phosphorus atoms and

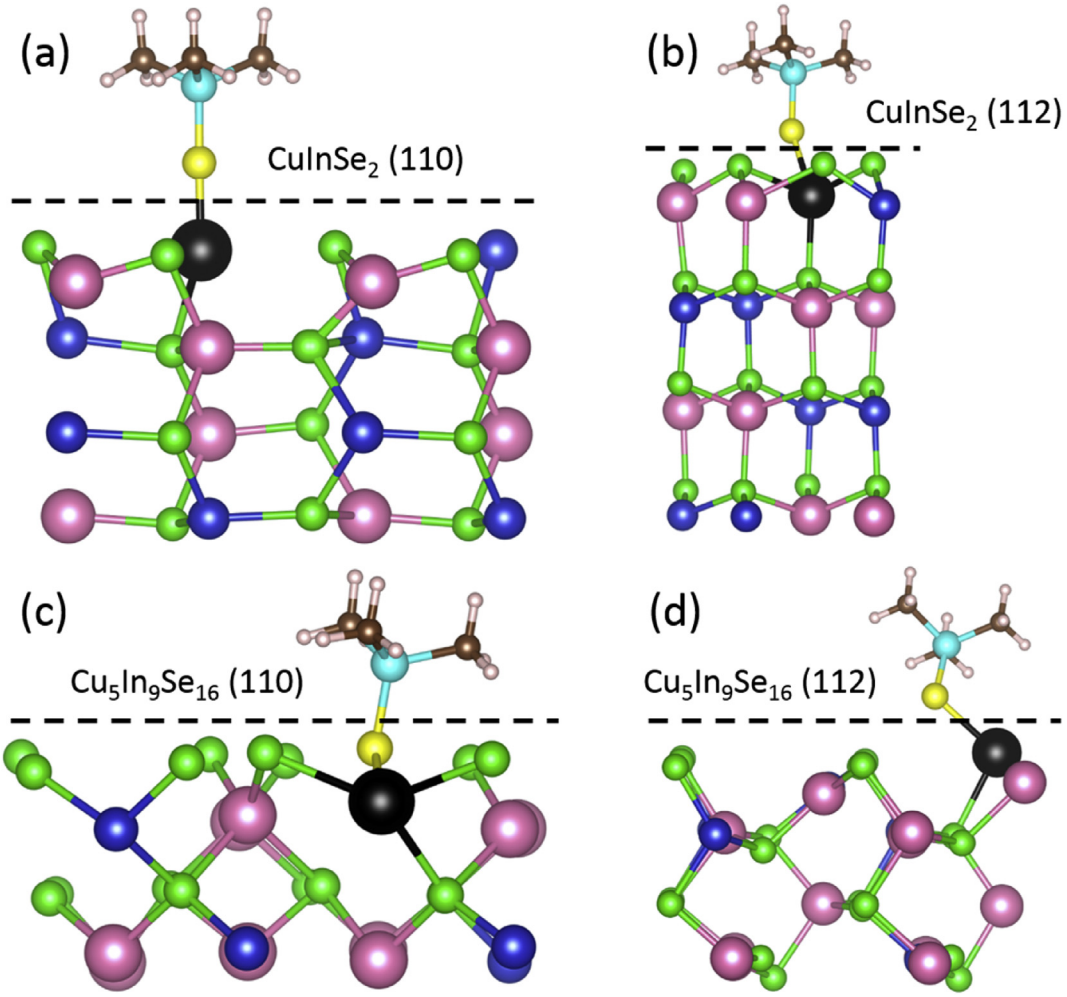

Fig. 7. Optimized surface geometry for (a) Cu-rich (110), (b) Cu-rich (112), (c) Cu-poor (110) and (d) Cu-poor (112) with $SP(CH_3)_3$ molecule, showing parts of the surfaces containing the Na_{Cu} substitution. Color scheme follows that of Fig. 4. Dashed lines show direction of the free surface. (For interpretation of the references to colour in this figure legend, the reader is referred to the web version of this article.)

dangling bonds near the film surface. Additional measurements at various passivation temperatures reveal that these peaks and the binding state of TOP:S on film surfaces are independent of passivation temperature (Fig. S1), which implies that the adsorption of TOP:S is not temperature-limited and is unlikely to fully account for the increase in PL response after passivation.

XPS measurements of surface Na *1s* peak follow trends similar to the PL response after TOP:S passivation. Fig. 2(a) shows a ~4.5 times increase in the passivated films compared with the as-fabricated ones after immersion in the TOP:S solution for 24 h, which remained relatively unchanged for longer passivation duration. Changes in the Na peaks appear to depend on the passivation temperature, with the enhancement from passivation at 120 °C over twice than that from passivation at RT (Fig. 2(b)). Those films that underwent only high-temperature annealing also show increased surface Na content (Fig. 2(c)), similar to existing literature reports [19,41]. However the improvement in Na content from the TOP/TOP:S passivation is over twice compared to just from high temperature annealing, and much higher than reference samples annealed at 120 °C which showed no change in Na content. Films passivated by TOP:S exhibit a higher Na peak compared to the TOP-passivated ones, which can be attributed to the formation of Na_2S, an energetically favorable species that is most notably known to passivate GaAs semiconductor devices [42,43]. Formation of Na_2S would also release the ligands within the TOP, which can in turn adhere to the surface via P bonds (Fig. 1(d)) to serve as a protective surface layer. This layer can be easily removed by solution rinsing before the deposition of additional layers during solar cell device fabrication [4,9].

Figs. 1 and 2 show that the PL and the XPS Na peak of CIS films follow similar trends after TOP:S passivation; both increasing monotonically with passivation temperature and passivation time, which for the latter reaches full saturation after 24 h of solution treatment. This suggests that the increase in surface Na content after passivation may contribute to the increased PL response. It has been suggested that Na can create surface dipole on CI(G)S thin films, which will lead to formation of depletion regions and changes in energy levels [7,44]; while recent work using scanning tunneling spectroscopy (STS) showed negative surface dipoles that are independent of surface Na content and attribute the depletion region formation to surface reconstruction [38], though it is generally accepted that increased alkali metal content can significantly alter CIS film surfaces. Our previous DFT calculations show high Na (and K) concentration at CIS film surface leads to energy level shifts [22], here we observed a decrease in the Fermi level of CIS surfaces relative to vacuum from 5.17 to 4.69 eV by measuring the ionization potential of the CIS films that were passivated at 120 °C for 24 h and the as-fabricated ones using a photoelectron

spectrometer (Fig. S4). Such shifts in energy levels serves to reduce surface recombination and to increase PL intensity, which would follow the increase in surface Na content, as shown in Fig. 2.

We propose two potential mechanisms to explain the greater surface concentrations of Na observed in the CIS films: (1) Na within the SLG substrate is dissolved in the TOP:S solution, after which it diffuses in the liquid state to re-deposit onto the film surface; or (2) the TOP:S passivation layer on the film surface provides the driving force for solid state diffusion of Na from the SLG substrate towards film surface. EDS analysis performed on a representative cross-section of each CIS film, shown in Fig. 3, reveals a "saddle-shaped" Na distribution in the as-fabricated films, and a close to linear bottom-to-top concentration gradient in the passivated films. Each measurement spanned an area of~70nm × 70 nm, which is sufficiently large to represent the characteristics of each film, whose morphology is inhomogeneous and has been shown to cause significant variances in localized spectroscopy measurements [11,45]. The overall increase in the surface Na content measured by EDS is ~20%, a substantially lower relative increase than the ~4× increase in XPS measurements. This is likely caused by the fabrication process of TEM samples, which exposes part of the surface Na in the Na_2S form to the atmospheric moisture and removes it. The Scanning TEM (STEM) probe can provide information on the Na distribution along the film thickness that cannot be obtained via surface measurements. The STEM-generated Na concentration profiles before and after passivation are shown in Fig. 3, their difference can be explained by the non-ideal film morphology as a function of film height. We propose that during the high temperature selenization process (550 °C), the Na enters the CIS films from SLG substrate and migrates towards the film surface via solid-state diffusion, which is impeded by the voids observed in all CIS films ~200 nm above the Mo layer, as shown in the STEM images in Fig. 3 and in our previous work [32]. It is likely that the transport of Na atoms through the pore-containing region is relatively sluggish and increases back to its original value in the more homogeneous portions of the film. As a result, the Na content is lower in the vicinity of the voids and, possibly, near other microstructural defects within the film. At equilibrium, all Na atoms entering the system are able to diffuse to the surface and through the void regions, which would set up a concentration gradient towards the surface, as shown in Fig. 3(b). The distinct change in the Na distribution profile after passivation supports the hypothesis that TOP:S passivation promotes Na diffusion towards film surface. XPS measurements on passivated films revealed a higher surface Na content (Fig. 2) compared to EDS, it is possible that the diffusion of Na from SLG substrate through TOP:S solution to the film surface also contributes to the increased surface Na concentration. The EDS measurements imply that solution-based Na, potentially in the form if Na_2S, can be easily removed from the film surface before the deposition of additional layers, which could be helpful since excessive Na has been shown to have a detrimental effect on device performance [15,18].

Altering surface properties via passivation has been shown to have significant impact on the diffusion in CI(G)S thin films [46,47]. Na has high affinity for TOP [48] and easily forms Na_2S [9] by binding with the active sulfur atom in TOP:S, the presence of the TOP:S passivation would likely enhance Na diffusion towards the film surface, providing an additional driving force for the solid state diffusion. During device fabrication, a CdS buffer layer is commonly deposited onto the CIS top surface. Our previous DFT studies showed that Na decreases conduction band offset (CBO) near the contact between CIS and CdS [22], and a higher Na content at the CIS surfaces would reduce the electron transport barrier across the interface. This could lead to better efficiency and improved V_{oc} of devices containing TOP:S passivated CI(G)S films [13,49].

4.2. Formation energy of Na in bulk CIS

We performed additional DFT calculations to investigate the effect of TOP:S on solid-state diffusion of Na along CIS film height. We considered the formation energy of different types of Na point defects in bulk CIS. The lower formation energy and greater stability of Na_{Cu} compared to other Na point defects shown in Fig. 4 agrees with previous calculations on CIS [22,33] and Cu-deficient $CuIn_5Se_8$ systems [50,51], which suggests that at equilibrium Na prefers to occupy Cu lattice sites in bulk CIS. This is corroborated by the experimental observations that the enhancement in CIS device performance from Na is more pronounced in Cu-poor CIS films [18,52]. The charge neutrality of Na_{Cu} formation leads to its insensitivity to the Fermi level. It has been suggested that the charge neutral Na_{Cu} does not introduce deep sites into the bandgap nor facilitates any other major alterations of the band structure [33]. Indeed this is what we find in our previous DFT studies, that it is more likely that populating the Na into Cu lattice sites will change the intrinsic defect mobility [33] while decreasing the CBO near the CIS—CdS interface [22].

4.3. Effects of surface condition on formation energy of Na_{Cu}

We determined the intrinsic diffusion pathways along CIS film height by calculating the formation energies of Na defects at the film surface. Fig. 6 shows that for each of the 4 types of surfaces, the formation energy for Na_{Cu} is lower than that in the bulk, with a 0.25 eV difference in the lowest energy Cu-poor (110) case. This will generate a driving force for Na diffusion from SLG substrate to the film surface, which corroborates the experimentally measured diffusion profile shown in Fig. 3.

It has been suggested that in CIS, the Na would be more readily incorporated into regions with lower Cu content [19,20], which is supported by bulk DFT calculations [13]. Our results indicate that both the surface concentration of Cu and the crystallographic surface orientation drive the Na_{Cu} defect formation. For example, under Cu-poor condition, the (110)-type surfaces have a 0.16 eV lower formation energy than the (112) surfaces; while under Cu-rich condition the formation energy for (110) surfaces is 0.03 eV higher compared that for (112). As the system moves towards equilibrium, Na will migrate towards the surface regions that have the lowest defect formation energy at the particular surface orientation and Cu content, which would lead to an inhomogeneous distribution of Na within the non-uniform film surface characteristic of sputtered CIS films [7,20,32]. This proposed mechanism agrees with previous reports [11] and is corroborated by the variations in measured surface Na content (Fig. 3).

4.4. Effect of TOP:S on surface formation energy of Na_{Cu}

Fig. 6 shows changes in the Na_{Cu} formation energy near the film surfaces in the vicinity of TOP:S molecules. We observed an overall decrease in the Na_{Cu} formation energy for all four surface cases; the formation energy decreased by 0.53 eV for Cu-poor (110) surface, by 0.96 for the Cu-rich (110) surface, and by 1.33 eV for the Cu-poor (112) surface with TOP:S treatment. This consistent lowering of the defect formation energy in the presence of TOP:S suggests that TOP:S passivation stabilizes Na defects in the vicinity of the surface, including the Na that diffuses from SLG substrate towards the surface through the film and the those that are dissolved in TOP:S solution from the SLG substrate and re-deposited onto the film surface. An important finding is that the reduction in Na_{Cu} formation energy in the presence of TOP:S passivation depends on the surface conditions with no clear preference for a particular surface orientation or Cu content. We found the largest drop in the

formation energy of 1.35eV to occur in the Cu-poor (112) surfaces; and the lowest such drop of 0.12 eV - for Cu-rich (112) surfaces. Fig. 7 shows the optimized geometries for various surface conditions and reveals a correlation between the defect formation energy and surface conditions. In all four cases, the surfaces were cleaved along [110] or [112] directions, terminating at a minimum energy surface. For the Cu-rich (110) and Cu-poor (112) surfaces, the Na_{Cu} site is in the topmost atomic layer within the free surface, which leads to its better positioning for interacting with the TOP:S molecule. For the Cu-rich (112) and Cu-poor (110) surfaces, the Na_{Cu} site is in the second atomic layer, buried by a topmost layer of Se atoms, which inhibits its access to the TOP:S molecule. In the Cu-poor (110) surfaces, the lattice is less densely packed due to the removal of the Cu atoms, which enables the S atom in the TOP:S molecule to penetrate into the surface, whereas in the Cu-rich (112) case, the interactions between a Na defect and the TOP:S molecule is hindered by surface geometry. This implies that Na defects in Cu-rich (112) surfaces are the least stable after passivation compared to all other studied surface conditions, which explains its lowest formation energy reduction.

5. Conclusions

We investigated the effects of TOP:S solution passivation on CIS thin films used in solar devices. The passivated films show a ~30× enhancement in photoluminescence (PL), which increases with passivation temperature to 120 °C and time up to 24 h. Surface XPS measurements on passivated samples reveal the formation of −S and −P bonds between the TOP:S and CIS and a >3-fold increase in the surface Na concentration. This is significantly higher than the increase from high-temperature annealing alone and follows the same trend with temperature and passivation time as PL. EDS analysis on the film cross-sections reveals a saddle-shaped Na concentration profile along the film height in the as-fabricated films and a bottom-to-top concentration gradient after passivation. We postulate that the higher Na content at the film surface creates a surface dipole that shifts the surface energy level and suppresses surface recombination in passivated films.

Our DFT calculations on stoichiometric and Cu-deficient systems reveal that.

(1) Na_{Cu} substitution is the most energetically favorable defect type in bulk CIS,
(2) Na_{Cu} defect formation energy is lower for the film surface compared with bulk and decreases after passivation,
(3) The defect energetics of Na before and after passivation are related to both the concentration of Cu at the surface and the crystallographic orientation of the surface, with Cu-poor surfaces having the lowest formation energy after passivation. (most favorable).

The experimental and computational results of this work indicate that TOP:S passivation introduces an additional driving force for Na diffusion within the solid CIS films and stabilizes the alkali metal defects, like Na and K, on CIS film surfaces, all of which lead to a greater surface Na content and reduced surface recombination in passivated films. This renders TOP:S a promising and effective passivation material for CIS-based photovoltaics. These studies provide fundamental insight and practical knowledge towards understanding the role and distribution of Na defects within CIS films and the effects of passivation, which will help create better solar cell devices.

Acknowledgment

The authors gratefully acknowledge the financial support of the National Science Council of Taiwan, R.O.C. through its grant no. NSC 101-3113-P-008-001.In addition HX and WAG received partial support from the US NSF.

Appendix A. Supplementary data

Supplementary data related to this article can be found at http://dx.doi.org/10.1016/j.actamat.2016.01.021.

References

[1] U. Rau, H.W. Schock, Electronic properties of Cu(In,Ga)Se 2 heterojunction solar cells-recent achievements, current understanding, and future challenges, Appl. Phys. A Mater. Sci. Process 69 (1999) 131–147, http://dx.doi.org/10.1007/s003390050984.
[2] P. Jackson, D. Hariskos, R. Wuerz, O. Kiowski, A. Bauer, T.M. Friedlmeier, et al., Properties of Cu(In,Ga)Se $_2$ solar cells with new record efficiencies up to 21.7%, Phys. Status Solidi Rapid Res. Lett. 9 (2015) 28–31, http://dx.doi.org/10.1002/pssr.201409520.
[3] A. Chirilă, S. Buecheler, F. Pianezzi, P. Bloesch, C. Gretener, A.R. Uhl, et al., Highly efficient Cu(In,Ga)Se2 solar cells grown on flexible polymer films, Nat. Mater. 10 (2011) 857–861, http://dx.doi.org/10.1038/nmat3122.
[4] M.T. Sheldon, C.N. Eisler, H.A. Atwater, GaAs passivation with trioctylphosphine sulfide for enhanced solar cell efficiency and durability, Adv. Energy Mater. 2 (2012) 339–344, http://dx.doi.org/10.1002/aenm.201100666.
[5] B. Vermang, V. Fjällström, J. Pettersson, P. Salomé, M. Edoff, Development of rear surface passivated Cu(In,Ga)Se2 thin film solar cells with nano-sized local rear point contacts, Sol. Energy Mater. Sol. Cells 117 (2013) 505–511, http://dx.doi.org/10.1016/j.solmat.2013.07.025.
[6] B. Vermang, J.T. Wätjen, V. Fjällström, F. Rostvall, M. Edoff, R. Kotipalli, et al., Employing Si solar cell technology to increase efficiency of ultra-thin Cu(In,Ga)Se 2 solar cells, Prog. Photovolt. Res. Appl. 22 (2014) 1023–1029, http://dx.doi.org/10.1002/pip.2527.
[7] W.-W. Hsu, J.Y. Chen, T.-H. Cheng, S.C. Lu, W.-S. Ho, Y.-Y. Chen, et al., Surface passivation of Cu(In,Ga)Se2 using atomic layer deposited Al2O3, Appl. Phys. Lett. 100 (2012) 023508, http://dx.doi.org/10.1063/1.3675849.
[8] H.C. Chen, S.W. Chou, W.H. Tseng, I.W.P. Chen, C.C. Liu, C. Liu, et al., Large auag alloy nanoparticles synthesized in organic media using a one-pot reaction: their applications for high-performance bulk heterojunction solar cells, Adv. Funct. Mater. 22 (2012) 3975–3984, http://dx.doi.org/10.1002/adfm.201200218.
[9] T.-H. Wong, C. Eisler, C. Chen, J. Bosco, D. Ryuzaki, W.-W. Hsu, et al., Surface Passivation of CuInSe2 with trioctylphosphine sulfide, MRS Bull. XVII (2013) 28.
[10] M. Kemell, M. Ritala, M. Leskelä, Thin film deposition methods for CuInSe 2 solar cells, Crit. Rev. Solid State Mater. Sci. 30 (2005) 1–31, http://dx.doi.org/10.1080/10408430590918341.
[11] D. Rudmann, G. Bilger, M. Kaelin, F.-J. Haug, H. Zogg, A.N. Tiwari, Effects of NaF coevaporation on structural properties of Cu(In,Ga)Se2 thin films, Thin Solid Films 431–432 (2003) 37–40, http://dx.doi.org/10.1016/S0040-6090(03)00246-3.
[12] D. Rudmann, A.F. da Cunha, M. Kaelin, F. Kurdesau, H. Zogg, A.N. Tiwari, et al., Efficiency enhancement of Cu(In,Ga)Se[sub 2] solar cells due to post-deposition Na incorporation, Appl. Phys. Lett. 84 (2004) 1129, http://dx.doi.org/10.1063/1.1646758.
[13] S.-H. Wei, S.B. Zhang, A. Zunger, Effects of Na on the electrical and structural properties of CuInSe2, J. Appl. Phys. 85 (1999) 7214, http://dx.doi.org/10.1063/1.370534.
[14] D. Rudmann, A.F. da Cunha, M. Kaelin, F.-J. Haug, H. Zogg, A.N. Tiwari, Effects of Na on the growth of Cu(In, Ga)Se2 thin films and solar cells, MRS Proc. 763 (2011) B1.9, http://dx.doi.org/10.1557/PROC-763-B1.9.
[15] K. Granath, M. Bodegård, L. Stolt, The effect of NaF on Cu (In, Ga) Se 2 thin film solar cells, Sol. Energy Mater. Sol. Cells 60 (2000) 279–293.
[16] P.-P. Choi, O. Cojocaru-Miredin, R. Wuerz, D. Raabe, Comparative atom probe study of Cu(In,Ga)Se2 thin-film solar cells deposited on soda-lime glass and mild steel substrates, J. Appl. Phys. 110 (2011) 124513, http://dx.doi.org/10.1063/1.3665723.
[17] P.-P. Choi, O. Cojocaru-Mirédin, R. Wuerz, Compositional gradients and impurity distributions in CuInSe 2 thin-film solar cells studied by atom probe tomography, Surf. Interface Anal. 44 (2012) 1386–1388, http://dx.doi.org/10.1002/sia.4948.
[18] S. Ishizuka, A. Yamada, M.M. Islam, H. Shibata, P. Fons, T. Sakurai, et al., Na-induced variations in the structural, optical, and electrical properties of Cu(In,Ga)Se[sub 2] thin films, J. Appl. Phys. 106 (2009) 034908, http://dx.doi.org/10.1063/1.3190528.
[19] V. Lyahovitskaya, Y. Feldman, K. Gartsman, H. Cohen, C. Cytermann, D. Cahen, Na effects on CuInSe[sub 2]: distinguishing bulk from surface phenomena,

J. Appl. Phys. 91 (2002) 4205, http://dx.doi.org/10.1063/1.1457539.
[20] S. Niki, M. Contreras, I. Repins, M. Powalla, K. Kushiya, S. Ishizuka, et al., CIGS absorbers and processes, Prog. Photovolt. Res. Appl. 18 (2010) 453–466, http://dx.doi.org/10.1002/pip.969.
[21] H. Xiao, J. Tahir-Kheli, W.A. Goddard, Accurate band gaps for semiconductors from density functional theory, J. Phys. Chem. Lett. 2 (2011) 212–217, http://dx.doi.org/10.1021/jz101565j.
[22] H. Xiao, W.A. Goddard, Predicted roles of defects on band offsets and energetics at CIGS (Cu(In,Ga)Se₂/CdS) solar cell interfaces and implications for improving performance, J. Chem. Phys. 141 (2014) 094701, http://dx.doi.org/10.1063/1.4893985.
[23] T.-T. Wu, J.-H. Huang, F. Hu, C. Chang, W.-L. Liu, T.-H. Wang, et al., Toward high efficiency and panel size 30×40cm2 Cu(In,Ga)Se2 solar cell: investigation of modified stacking sequences of metallic precursors and pre-annealing process without Se vapor at low temperature, Nano Energy 10 (2014) 28–36, http://dx.doi.org/10.1016/j.nanoen.2014.07.018.
[24] T.-T. Wu, F. Hu, J.-H. Huang, C. Chang, C. Lai, Y.-T. Yen, et al., Improved efficiency of a large-area Cu(In,Ga)Se₂ solar cell by a nontoxic hydrogen-assisted solid Se vapor selenization process, ACS Appl. Mater. Interfaces 6 (2014) 4842–4849, http://dx.doi.org/10.1021/am405780z.
[25] O. Madelung, Semiconductors: Data Handbook, Springer, Berlin Heidelberg, 2004, http://dx.doi.org/10.1007/978-3-642-18865-7.
[26] A.D. Becke, Density-functional thermochemistry.III. The role of exact exchange, J. Chem. Phys. 98 (1993) 5648, http://dx.doi.org/10.1063/1.464913.
[27] R. Dovesi, V.R. Saunders, C. Roetti, R. Orlando, C.M. Zicovich-Wilson, F. Pascale, B. Civalleri, K. Doll, N.M. Harrison, I.J. Bush, P. D'Arco, M. Llunell, CRYSTAL 2009 User's Manual, University of Torino, Torino, 2009.
[28] C.F. Melius, W.A. Goddard, Ab initio effective potentials for use in molecular quantum mechanics, Phys. Rev. A 10 (1974) 1528–1540, http://dx.doi.org/10.1103/PhysRevA.10.1528.
[29] C.F. Melius, B.D. Olafson, W.A. Goddard, Fe and Ni AB initio effective potentials for use in molecular calculations, Chem. Phys. Lett. 28 (1974) 457–462, http://dx.doi.org/10.1016/0009-2614(74)80079-5.
[30] W.J. Stevens, M. Krauss, H. Basch, P.G. Jasien, Relativistic compact effective potentials and efficient, shared-exponent basis sets for the third-, fourth-, and fifth-row atoms, Can. J. Chem. 70 (1992) 612–630, http://dx.doi.org/10.1139/v92-085.
[31] H.J. Monkhorst, J.D. Pack, Special points for Brillouin-zone integrations, Phys. Rev. B 13 (1976) 5188–5192, http://dx.doi.org/10.1103/PhysRevB.13.5188.
[32] S. Luo, J.-H. Lee, C.-W. Liu, J.-M. Shieh, C.-H. Shen, T.-T. Wu, et al., Strength, stiffness, and microstructure of Cu(In,Ga)Se2 thin films deposited via sputtering and co-evaporation, Appl. Phys. Lett. 105 (2014) 011907, http://dx.doi.org/10.1063/1.4890086.
[33] L.E. Oikkonen, M.G. Ganchenkova, A.P. Seitsonen, R.M. Nieminen, Effect of sodium incorporation into CuInSe2 from first principles, J. Appl. Phys. 114 (2013) 083503, http://dx.doi.org/10.1063/1.4819105.
[34] M.V. Yakushev, A.V. Mudryi, V.F. Gremenok, V.B. Zalesski, P.I. Romanov, Y.V. Feofanov, et al., Optical properties and band gap energy of CuInSe2 thin films prepared by two-stage selenization process, J. Phys. Chem. Solids 64 (2003) 2005–2009, http://dx.doi.org/10.1016/S0022-3697(03)00089-1.
[35] S.H. Kang, Y.-K. Kim, D.-S. Choi, Y.-E. Sung, Characterization of electrodeposited CuInSe2 (CIS) film, Electrochim. Acta 51 (2006) 4433–4438, http://dx.doi.org/10.1016/j.electacta.2005.12.021.
[36] S.R. Kodigala, Cu(In1-xGax)Se2 Based Thin Film Solar Cells, Academic Press, 2011.
[37] J. Jaffe, A. Zunger, Defect-induced nonpolar-to-polar transition at the surface of chalcopyrite semiconductors, Phys. Rev. B 64 (2001) 241304, http://dx.doi.org/10.1103/PhysRevB.64.241304.
[38] S. Bröker, D. Kück, A. Timmer, I. Lauermann, B. Ümsür, D. Greiner, et al., Correlating the local defect-level density with the macroscopic composition and energetics of chalcopyrite thin-film surfaces, ACS Appl. Mater. Interfaces 7 (2015) 13062–13072, http://dx.doi.org/10.1021/acsami.5b03260.
[39] H. Mönig, D. Lockhorn, N. Aghdassi, A. Timmer, C. a Kaufmann, R. Caballero, et al., Heat induced passivation of CuInSe 2 surfaces: a strategy to optimize the efficiency of chalcopyrite thin film solar cells? Adv. Mater. Interfaces 1 (2014) http://dx.doi.org/10.1002/admi.201300040.
[40] B. Vermang, V. Fjallstrom, X. Gao, M. Edoff, Improved rear surface passivation of Cu(In,Ga)Se2 solar cells: a combination of an Al2O3 rear surface passivation layer and nanosized local rear point contacts, IEEE J. Photovolt. 4 (2014) 486–492, http://dx.doi.org/10.1109/JPHOTOV.2013.2287769.
[41] A. Rockett, M. Bodegard, K. Granath, L. Stolt, Na incorporation and diffusion in CuIn(1-x)Ga(x)Se2, in: Conf. Rec. Twenty Fifth IEEE Photovolt. Spec. Conf. - 1996, 1996, pp. 985–987, http://dx.doi.org/10.1109/PVSC.1996.564295.
[42] C.J. Sandroff, R.N. Nottenburg, J.-C. Bischoff, R. Bhat, Dramatic enhancement in the gain of a GaAs/AlGaAs heterostructure bipolar transistor by surface chemical passivation, Appl. Phys. Lett. 51 (1987) 33, http://dx.doi.org/10.1063/1.98877.
[43] E.A. Miller, G.L. Richmond, Photocorrosion of n-GaAs and passivation by Na 2 S: a comparison of the (100), (110), and (111)B faces, J. Phys. Chem. B 101 (1997) 2669–2677, http://dx.doi.org/10.1021/jp962852k.
[44] B.L. Kronik, D. Cahen, H.W. Schock, Effects of sodium on polycrystalline Cu(In,Ga)Se 2 and its solar cell performance, Adv. Mater. 10 (1998) 31–36, http://dx.doi.org/10.1002/(SICI)1521-4095(199801)10, 1<31::AID-ADMA31>3.0.CO;2–3.
[45] T. Nakada, H. Ohbo, M. Fukuda, A. Kunioka, Improved compositional flexibility of Cu(In,Ga)Se2-based thin film solar cells by sodium control technique, Sol. Energy Mater. Sol. Cells 49 (1997) 261–267, http://dx.doi.org/10.1016/S0927-0248(97)00202-X.
[46] K. Hiepko, J. Bastek, R. Schlesiger, G. Schmitz, R. Wuerz, N. a. Stolwijk, Diffusion and incorporation of Cd in solar-grade Cu(In,Ga)Se2 layers, Appl. Phys. Lett. 99 (2011) 234101, http://dx.doi.org/10.1063/1.3665036.
[47] J. Bastek, N.A. Stolwijk, R. Wuerz, A. Eicke, J. Albert, S. Sadewasser, Zinc diffusion in polycrystalline Cu(In,Ga)Se2 and single-crystal CuInSe2 layers, Appl. Phys. Lett. 101 (2012) 074105, http://dx.doi.org/10.1063/1.4745927.
[48] Y. Komatsu, Y. Fujiki, Y. Michiue, Y. Yajima, T. Sasaki, Solvent extraction separation of alkaline earth metal ions with thenoyltrifluoroacetone and trioctylphosphine oxide in carbon tetrachloride, Solvent Extr. Ion. Exch. 9 (1991) 471–479, http://dx.doi.org/10.1080/07366299108918065.
[49] Q. Guo, G.M. Ford, R. Agrawal, H.W. Hillhouse, Ink formulation and low-temperature incorporation of sodium to yield 12% efficient Cu(In,Ga)(S,Se) 2 solar cells from sulfide nanocrystal inks, Prog. Photovolt. Res. Appl. 21 (2013) 64–71, http://dx.doi.org/10.1002/pip.2200.
[50] J. Kiss, T. Gruhn, G. Roma, C. Felser, Theoretical study on the structure and energetics of Cd insertion and Cu depletion of CuIn5Se8, J. Phys. Chem. C 117 (2013) 10892–10900, http://dx.doi.org/10.1021/jp312467f.
[51] J. Kiss, T. Gruhn, G. Roma, C. Felser, Theoretical study on the diffusion mechanism of Cd in the Cu-poor phase of CuInSe 2 solar cell material, J. Phys. Chem. C 117 (2013) 25933–25938, http://dx.doi.org/10.1021/jp4087877.
[52] S. Ishizuka, A. Yamada, K. Matsubara, P. Fons, K. Sakurai, S. Niki, Alkali incorporation control in Cu(In,Ga)Se[sub 2] thin films using silicate thin layers and applications in enhancing flexible solar cell efficiency, Appl. Phys. Lett. 93 (2008) 124105, http://dx.doi.org/10.1063/1.2992061.